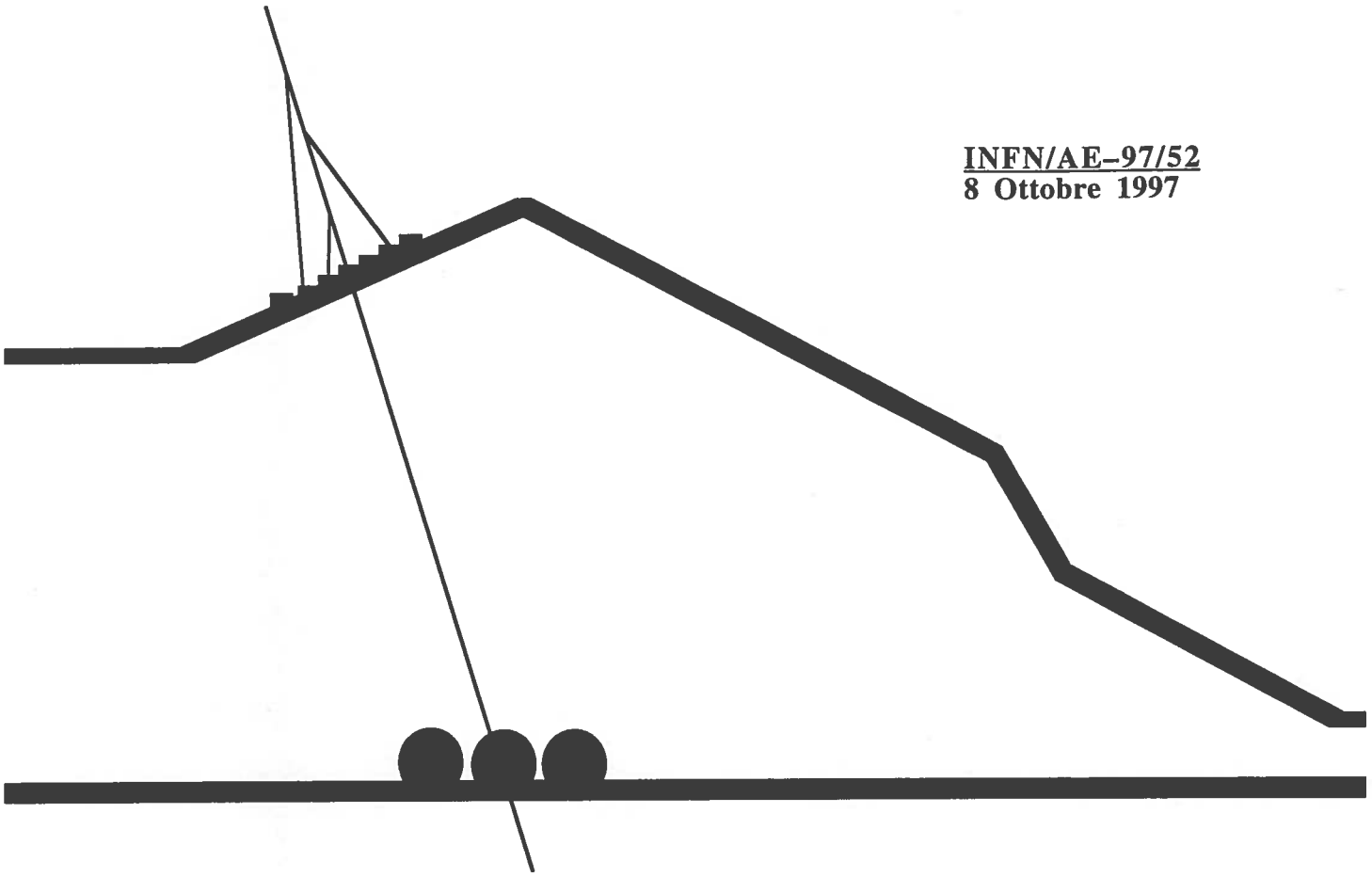

INFN/AE–97/52
8 Ottobre 1997

# Underground Neutron Spectrometry with a Liquid Scintillator Detector

F. Arneodo, F. Cavanna, S. Parlati, G. Piano Mortari, C. Rossi, E. Tatananni,
M. Verdecchia, A. Borio di Tigliole, A. Cesana, M. Terrani, R. Dolfini,
R. Nardò, A. Rappoldi, G.L. Raselli, M. Rossella, C. Vignoli

**INFN – Laboratori Nazionali del Gran Sasso**

*Published by* ***SIS–Pubblicazioni***
*dei Laboratori Nazionali di Frascati*

**INFN – Istituto Nazionale di Fisica Nucleare**
**Laboratori Nazionali del Gran Sasso**

**INFN/AE–97/52**
**8 Ottobre 1997**

# Underground neutron spectrometry with a liquid scintillator detector

F. Arneodo, F. Cavanna, S. Parlati, G. Piano Mortari, C. Rossi, E. Tatananni*, M. Verdecchia

*Dipartimento di Fisica dell'Università dell'Aquila and INFN (LNGS) - Gruppo Collegato dell'Aquila*, Via Vetoio, I-67010 L'Aquila, Italy

A. Borio di Tigliole, A. Cesana, M. Terrani

*Dipartimento di Ingegneria Nucleare del Politecnico di Milano and INFN - Sezione di Milano*, via Ponzio 34/3, I-20123 Milano, Italy

R. Dolfini, R. Nardò, A. Rappoldi, G.L. Raselli, M. Rossella, C. Vignoli.

*Dipartimento di Fisica Teorica e Nucleare dell'Università di Pavia and INFN- Sezione di Pavia*, Via Bassi 6, I-27100 Pavia, Italy

## Abstract

An array of neutron counters, filled with hydrogenated liquid scintillator, is operating in the hall-C of the Gran Sasso Laboratory. The detector discriminates recoiling protons from the electrons produced by γ-rays. It is particularly designed to operate with very low neutron fluxes in the presence of intense γ-ray background. We apply two different Pulse Shape Discrimination (PSD) methods and we require a delayed coincidence with an electron signal, produced in the interaction of the γ-rays following the neutron capture. We present and discuss the results obtained with a preliminary part of the detector. A very small contamination of α emitters inside the scintillation medium (about $4 \cdot 10^{8}$ atoms of $^{226}Ra$ per litre) can explain the presence of non neutron signals, surviving the PSD selection. The subtraction of these events, requiring the neutron capture coincidence, reduces the measured flux to about $10^{-2}$ neutron per squared meter per second ($E \geq 1$ MeV), which is compatible with the published data. In the full detector we expect to collect a reasonable number of unambiguous neutron signals, sufficient to reconstruct the neutron energy spectrum in the range 1-10 MeV.

---

* Permanent address: INFN - Laboratori Nazionali del Gran Sasso, s.s. 17-bis Km 18.910, I 67010 ASSERGI (AQ), Italy

## 1. Introduction

The ICARUS detector [1] will offer "bubble chamber like" events for the study of the $^{8}B$ solar neutrino energy spectrum at the Gran Sasso Laboratory (LNGS). The energy associated to these events is low (few MeV) and they are so rare that the environmental radioactivity could represent a serious background. A study of the solar neutrino signal vs. background, based on the existing data on natural radioactivity measured in the LNGS underground laboratory [2] has been performed for by means of a dedicated Montecarlo simulation [3]. The predictions of this MC study show that the main contribution to the background comes from the neutron field in the experimental site, despite its very low intensity. Owing to this fact, the experimental errors on the published data are necessarily important, in particular for what concerns the energy distribution. This consideration strongly suggests to collect new data on the neutron field in the LNGS hall C, where the ICARUS detector will operate, in order to confirm experimentally the reliability of the solar neutrino experiment.

The measurement of the proton recoil energy in an hydrogenated liquid scintillator is a very sensitive technique in fast neutron spectrometry. The Pulse Shape Discrimination (PSD) technique furnishes an efficient method to discriminate neutrons from other particles (gamma, alpha, etc.). A liquid scintillator detector for neutron spectrometry in the Gran Sasso underground laboratory has been designed and built by the ICARUS Collaboration. The sensitive volume is made out of 32 one-litre-cells to fulfill minimal detection efficiency requirements. It employs two independent stages of PSD. The scintillator cells and the PSD electronics are home designed and realized [4].

The first two cells of the final 32-cells detector are working and collecting data since December 1996 in hall-C at the LNGS. Results from the analysis of these data are reported in this paper. We have found that some background signals, not compatible with neutron interactions, survive the selection from the two independent stages of PSD in use. The nature of these events has been considered in details and completely understood. In order to reject this noise an additional criterion for unambiguous neutron identification is needed. Therefore, we require the detection of a delayed gamma, produced by the capture of the interacting neutron after thermalization [5]. In order to enhance the capture probability the cells are wrapped with cadmium foils.

## 2. Pulse Shape Discrimination

The decay time of the light output of a scintillator depends on the ionization density of the interacting particle. The fast decay component dominates in the light produced by low ionizing particles such as electrons, whereas the slow component becomes more important for highly ionizing particles like the protons generated in the elastic scattering of neutrons on hydrogen. We use two different ways to

distinguish between proton signals, from neutron interactions, and electrons, from gamma interactions:

a) The Zero-Crossing-Time method (ZCT): the anode signal (from the PMT's viewing the light output from the cells) is integrated and differentiated so that the decay time of the input pulse determines the zero-crossing point of the output pulse. The measure of this time allows to discriminate between fast and low component, namely the particle type.

b) The Digital Charge Comparison (DCC) method: we measure the total charge, obtained by integration of the whole pulse, and the delayed charge resulting by the integration over the pulse tail [6]. Again, the off-line comparison between these two charges allows to discriminate between neutron and gamma.

The DCC method yields digital output signals, read out with conventional electronics. On the other hand, the ZCT method in our case needs non standard electronics. A dedicated electronic chain has been developed to issue the on-line information that can be promptly used to define a trigger for the data acquisition system. The possibility to have a PSD information at the trigger level is fundamental to enhance the separation between neutron and gamma events and consequently to lower the undesired gamma ray contribution to the acquisition rate.

## 3. The detector

The preliminary data presented in this paper have been recorded with part of the final neutron detector, during about 3 mounts of data taking. Namely, with the first two cells which have been built and filled with a selected liquid scintillator, *BicronBC501A* [7]. In Par. 3.1, we briefly report some constructive details of the cells.

### 3.1 *The liquid scintillator cells.*

Each cell is composed by an inner, white Teflon tube ($T_I$) for the light diffusion. The dimensions of the $T_I$ tube are: length 500mm, internal diameter 50mm, thickness 1.5mm [corresponding to an internal volume of 982 cc]. The $T_I$ tube is inserted into a coaxial stainless steel tube ($T_E$) (internal diameter 59mm, thickness 1.5mm). When the cell is in the horizontal position, $T_I$ is full of liquid while the hollow space between $T_I$ and $T_E$ is only partially filled by the liquid, in order to provide a sufficient empty volume for possible thermal expansion ($\Delta T_{max} = 30^o$).

The $T_E$ tube ends up with two Al flanges sealing a glass optical window (thickness 6mm). Two fast PMTs (2" diameter, *EMI 9964 KB03*) are attached directly to both ends of each cell. The coupling between the photomultiplier and the glass window is provided by silicon grease. The tightness of the cell is guaranteed by Teflon O-rings. The external part of the flanges are threaded in order to hold a Al tube supporting the photomultiplier and its basis (*NES 4238*).

The tightness of the cell is checked with a vacuum pump down to $10^{-3}$ mbar before filling.

A Cadmium foil covers the external surface of the $T_E$ tube, to provide a high cross section target for thermalised neutrons. A protective Teflon painting prevents Cd dust spreading in atmosphere.

3.2 *The electronic setup.*

The first pulse above threshold following the elastic (n,p) collision of a fast neutron entering one of the cells, opens a 10 μs gate. During this time the apparatus waits for the detection of a γ-ray signal following the capture of the same neutron after thermalization. If this happens, the event is recognized as a neutron interaction. This further constraint on neutron selection has been not employed in the two cell array, due to low statistical significance. The fig. 1 shows a block diagram of the electronic set-up used for the two-cells detector. There are three different electronic stages: 1) the front-end electronics, 2) the data acquisition system and 3) the timing system.

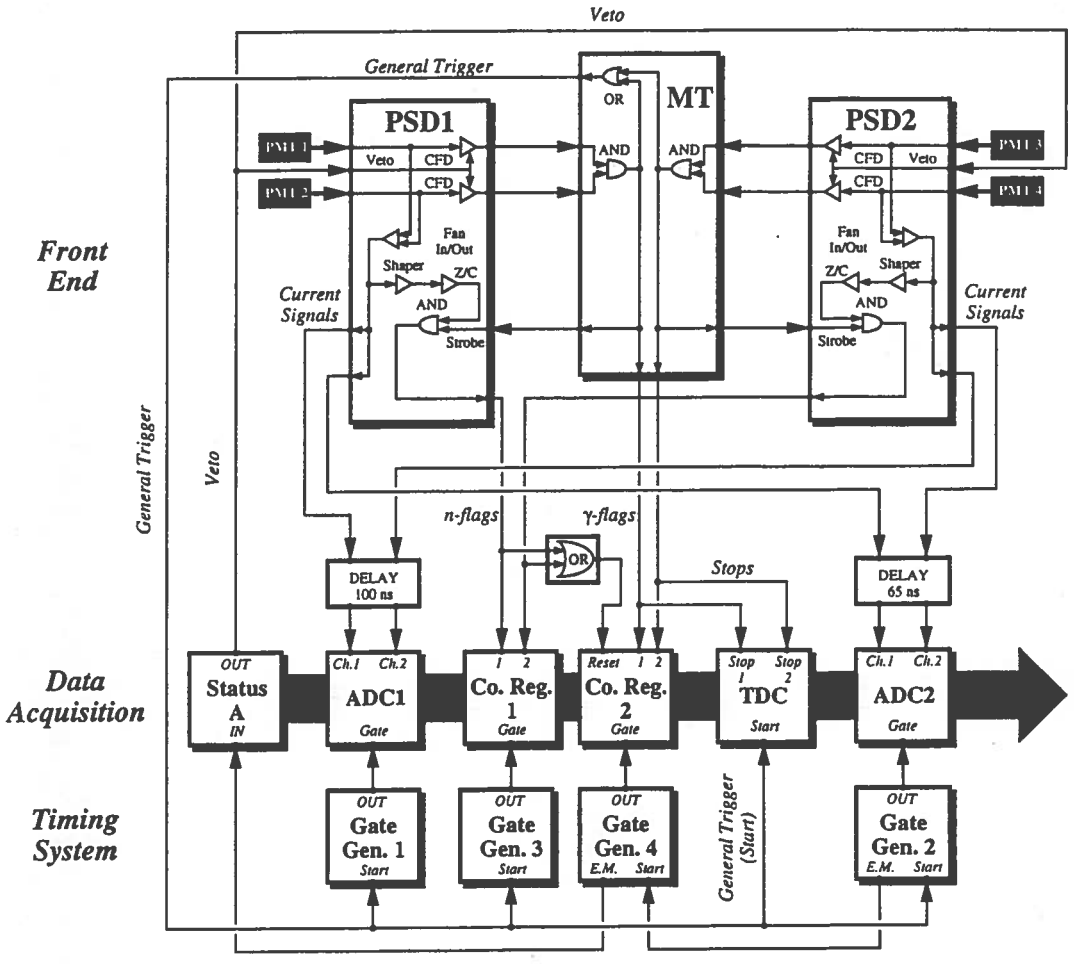


Fig. 1 The electronic set up.

*Front-end electronics*

The front-end electronics is especially designed for this experiment and makes use of two full-integrated PSD Units and two Meantimer (MT) channels.

The PSD Units, directly connected to the PMT outputs perform a linear sum of the anode signals, to reduce the dependence of the pulse shape from the interaction coordinate along the counter axis. An internal constant fraction discriminator selects the events above threshold. Each unit generates an identification logic signal (n-flag) if the zero crossing time of the event corresponds to a neutron interaction and provides twofold Current Signals, to be used for total and delayed charge measurement.

The Meantimer module generates a common signal for the two cells, to be used as the General Trigger of the data acquisition system. Moreover it provides time compensated logic signals in two independent lines, one for each counter. These are used to measure the delay between consecutive interactions of the same primary neutron (Stop Signal) and to recognize the delayed gamma rays ($\gamma$-flags).

*Data acquisition system*

The data acquisition system consists of the following CAMAC electronics:

1) two TDC channels (10 bit, 50 ps resolution) used for time delay measurement,

2) four FERA ADC (11 bit) channels for total and delayed charge sampling,

3) four coincidence registers (Co.Reg.) channels: two used to store the presence of an n-flag, for each counter, and two to store the delayed $\gamma$'s.

4) one STATUS A channel to determine the status of the data acquisition.

*Timing system*

Four gate generators enable the data acquisition units with the correct time sequence. A fast neutron entering the detector will induce n-type signals during the thermalization in the liquid scintillator, followed by a delayed capture $\gamma$ signal. The first pulse starts the timing system that generates a 10 $\mu$s cycle of logic signals, as shown in fig. 2.

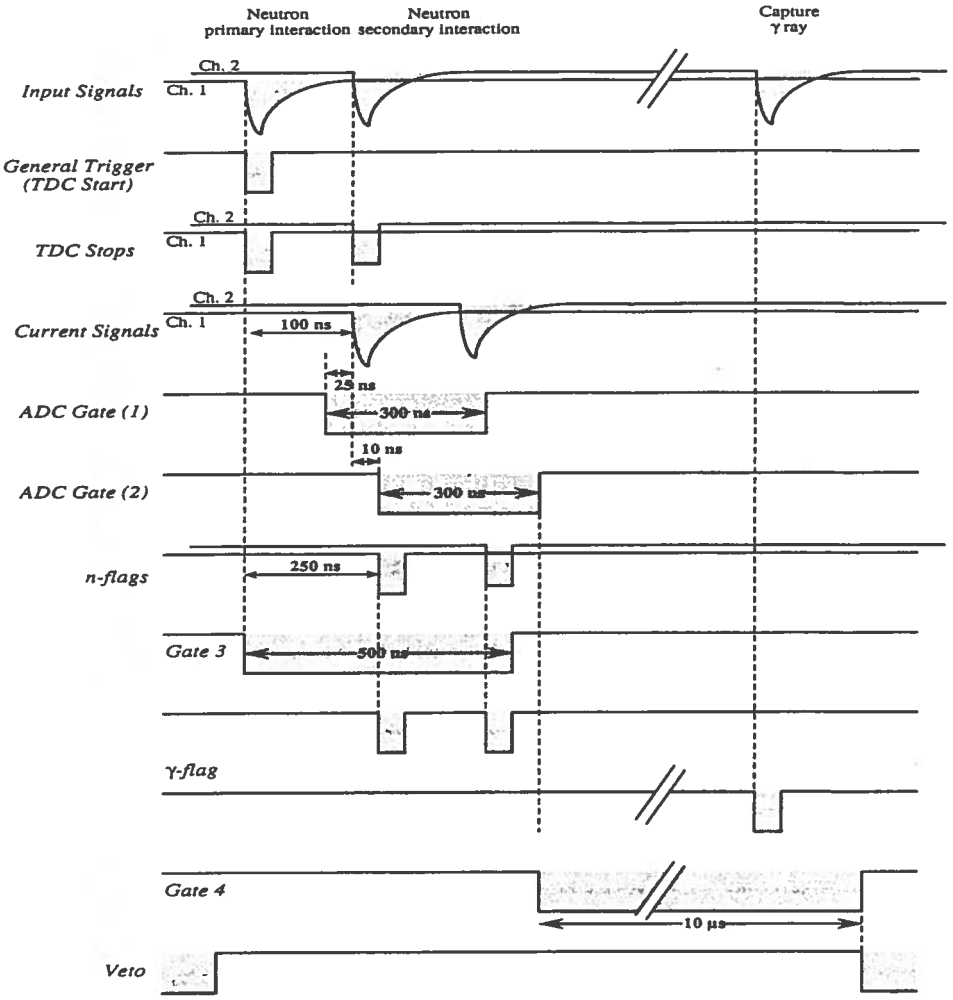


Fig. 2 The timing system.

Since non–updating electronics is used, secondary neutron interactions do not affect the correct timing generation.

The general trigger starts the timing chain. Every neutron interaction in a counter gives the Stop to the corresponding TDC channel. The stored information will allow, in the final detector, the reconstruction of the neutron path. In the present detector this information simply says which was the first detector to be fired.

The window (Gate 1) for the ADC modules, used for the total charge measurement, is opened 25 ns before the arrive of the leading edge of the current pulse to the ADC input. The width (300 ns) is long enough to wholly integrate the PMT current pulses.

A 300 ns window (Gate 2) is opened for the delayed charge integration 10 ns after the current pulse leading edge at the ADC input. A 500 ns gate (Gate 3) enables the coincidence register to store the n-flags presence. A 10 μs gate (Gate 4) is opened to store γ-flags; this time is needed for a neutron to thermalize inside the scintillator and to be captured by the cadmium foil.

The two input channels of the first Co.Reg are directly connected to the PSD n-flag outputs while the two input channels of the second Co.Reg are directly

connected to the MT outputs. To assure the correct time sequence (neutron-delayed gamma) the PSD outputs reset the second coincidence register. At the end of the timing cycle the STATUS A unit vetoes the electronics during the data taking.

In the read-out system the event acquisition is determined by the presence of a LAM signal generated by the STATUS A module. The on-line program checks the presence of the LAM signal in the first Co.Reg. When this LAM is set a neutron interaction has occurred and the data readout starts. The General Memory Clear follows, the Veto signal is switched off, and the electronics is ready for a new data acquisition cycle.

## 4. Detector performances

We present the energy calibrations and the detector response to different radiations.

### 4.1 *Energy calibration*

We obtain the energy calibration in "MeV electron equivalent" of the ADC counts from the position of the Compton edges, obtained with monoenergetic gamma sources. The calibration procedure, as explained in details in [8] takes into account a MonteCarlo pulse height spectrum of the gamma source, smeared with a gaussian response function representing the detector resolution. We obtain the calibration parameters by comparison amongst the simulated and measured spectra. The best fit to the collected data gives:

$$E\,(MeV\,ee) \;=\; 0.00204 \cdot C_{ADC} - 0.0095.$$

### 4.2 *Neutron and gamma sources*

A series of tests and measurements, by exposing the counters to Am-Be and $^{252}Cf$ sources (simultaneously providing neutrons and gamma's), have been performed before the installation in the underground experimental site. In Fig. 3 we show the zero-crossing time distribution of neutrons and gamma's.

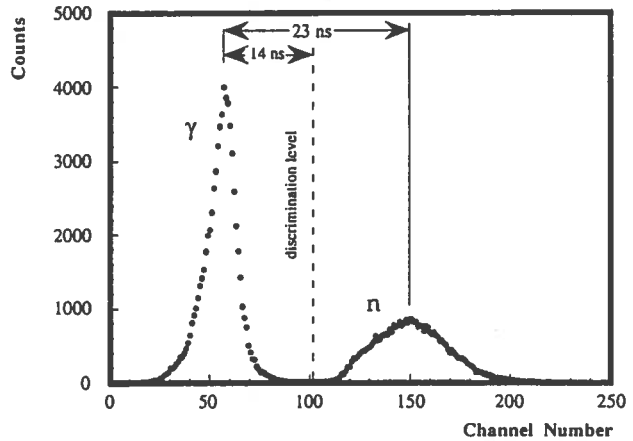


Fig. 3. ZCT distribution, 0.250 ns/channel. The energy threshold is fixed at 0.2 MeV (electron equivalent). The dashed line represents the chosen discrimination level between neutron and gamma.

The two peaks are very well separated and the discrimination level can be easily chosen (the dashed line in the figure). The signals above this level give the n-flag output of the PSD module. In Fig. 4 we show the correlation between delayed and total charge.

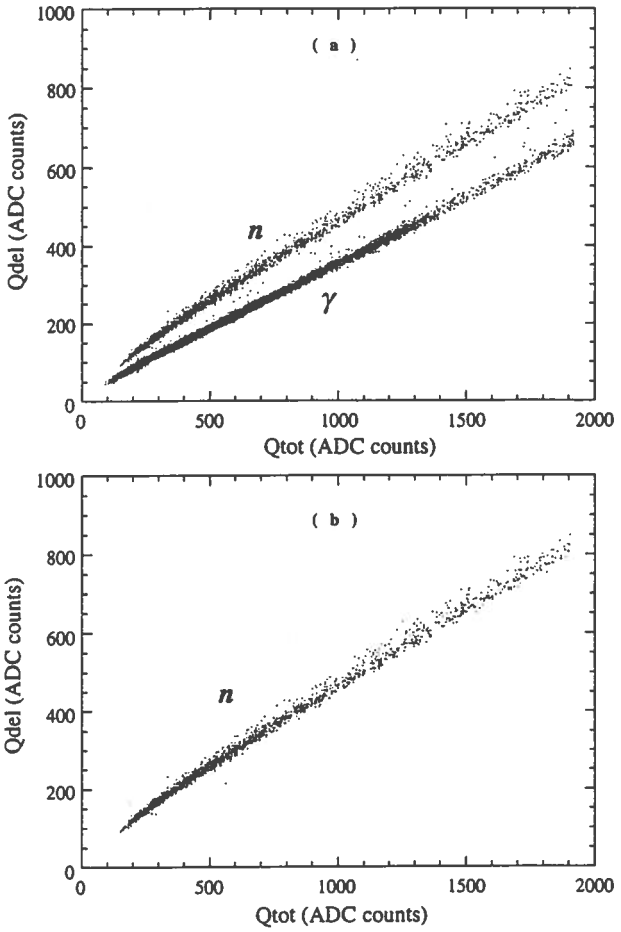


Fig. 4 a. Neutron and gamma source. Delayed Vs total charge, without n-flag selection of the PSD module. The energy threshold is fixed at 0.2 MeV e.e.

4 b. The same of Fig 5-a but with n-flag (ZCT) selection.

The additional DCC (digital charge comparison) selection can be defined by appropriate cuts on this plane. With this source the fraction of the γ-rays (DCC selected) surviving the ZCT n-flag selection is about $10^{-3}$ with 0.2 MeV_ee energy threshold. The fraction of neutrons (ZCT selected) but recognized as γ by DCC selection is about $8 \times 10^{-3}$. This fraction depends on the actual settings of the ZCT discrimination level.

4.3 *Cosmic radiation*

The events, recorded with the detector exposed to the cosmic rays at sea-level in an above ground laboratory, present a large fraction of overflows in the charge scale (gamma branch), due to the muons crossing the sensible volume.

In Fig. 5 we compare the energy distribution (MeV_electron equivalent) of neutrons produced by the $^{252}Cf$ spontaneous fission source, with the distribution of neutrons present in the cosmic radiation at sea-level. The shapes of the two distributions appear to be quite similar at low energy. It is interesting to observe that the energy spectrum of this spontaneous fission source is expected to be similar to that of the neutron field in the underground laboratory.

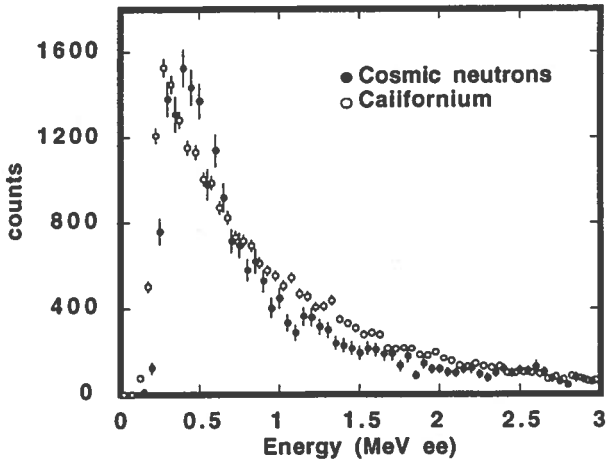


Fig 5 Energy spectrum of proton recoils. Californium source and cosmic neutron at sea level.

**5. Underground operating conditions**

We need a detailed knowledge of the neutron energy distribution for a very low underground field (at least 3 orders of magnitude lower than that one present at the sea level and several order of magnitude lower than those usually considered in neutron spectroscopy).

In the following paragraphs we present some results using the two-cells array mounted in the LNGS hall- C.

5.1 *Accidental γ-rays coincidences*

We performed a test run to measure the rate of γ-ray signals. This information allows us to evaluate the contamination of the random γ-ray coincidences in the neutron selected sample, and hence to estimate the systematic error and the lower limit for the measurability of the neutron flux. We measured a gamma event rate of 100 Hz (200 KeV_ee threshold), leading to a small but significant contamination of neutron-like signals due to accidental γ-rays coincidences in the 300 ns ADC gate. The consequent accidental rate should be $3x10^{-5}$ to be compared with the rate of proton recoils expected from extrapolation of the published data on the neutron flux

at LNGS: about $5 \times 10^{-5}$ Hz. Even though this contamination will be partly removed by requiring the coincidence of a proton pulse with a delayed $\gamma$-ray pulse, produced in the thermal neutron capture, it is advisable to improve this signal to noise ratio. For this reason we surrounded the detector with a 5 cm Cu shield which cuts down the gamma rate to 9 Hz, leading to an accidental rate of about $2.7 \times 10^{-6}$ Hz (a factor 20 lower than the expected neutron rate). The coincidence rate of these accidental signals and the delayed $\gamma$ from the neutron capture is quite negligible.

### 5.2 *PSD neutron selection*

In Fig. 6 we display the delayed versus total charge plot of the events triggered by the ZCT neutron-flag. The points in the upper part of this plane constitute the PSD neutron sample fulfilling both the ZCT and DCC constraints. The rate of these "neutron candidate" was surprisingly large: $3 \times 10^{-3}$ Hz, i.e. from one to two orders of magnitude greater than the expected one. The energy spectrum of the PSD neutron candidates is shown in Fig. 7a. It is definitively different from the expected proton recoils spectrum produced in neutron elastic scattering. This statement is also supported by the comparison with the Californium recoils spectrum.

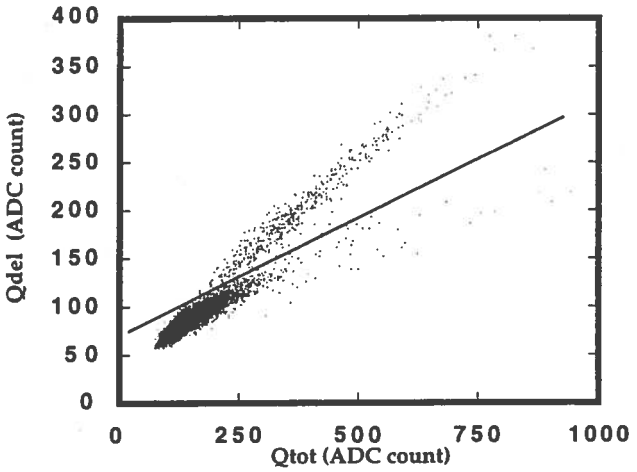


Fig. 6 Delayed versus total charge with the detector surrounded by 5 cm Cu shield. The continuous line represents the cut used in the DCC selection.

Other authors [9] observed events with the same characteristics, using a similar liquid scintillator detector. They concluded that the recorded signals were not due to neutron interactions. However, to our knowledge a conclusive investigation about their true nature was never performed.

Due to their frequency, these spurious events could seriously perturb our measure if not correctly understood. An accurate investigation of the electrical network noise and of the electronic chain was unfruitful to explain their origin. With a 0.3 litre cell manufactured by *Bicron* we found indeed presence of the same kind of unexpected signals. However, the count rate resulted not related to the cell volume or surface. Moreover, the rate was insensitive to the presence of various

kind of shields (copper, lead and/or paraffin) around the detector. This facts led us to exclude particles coming from outside the cell.

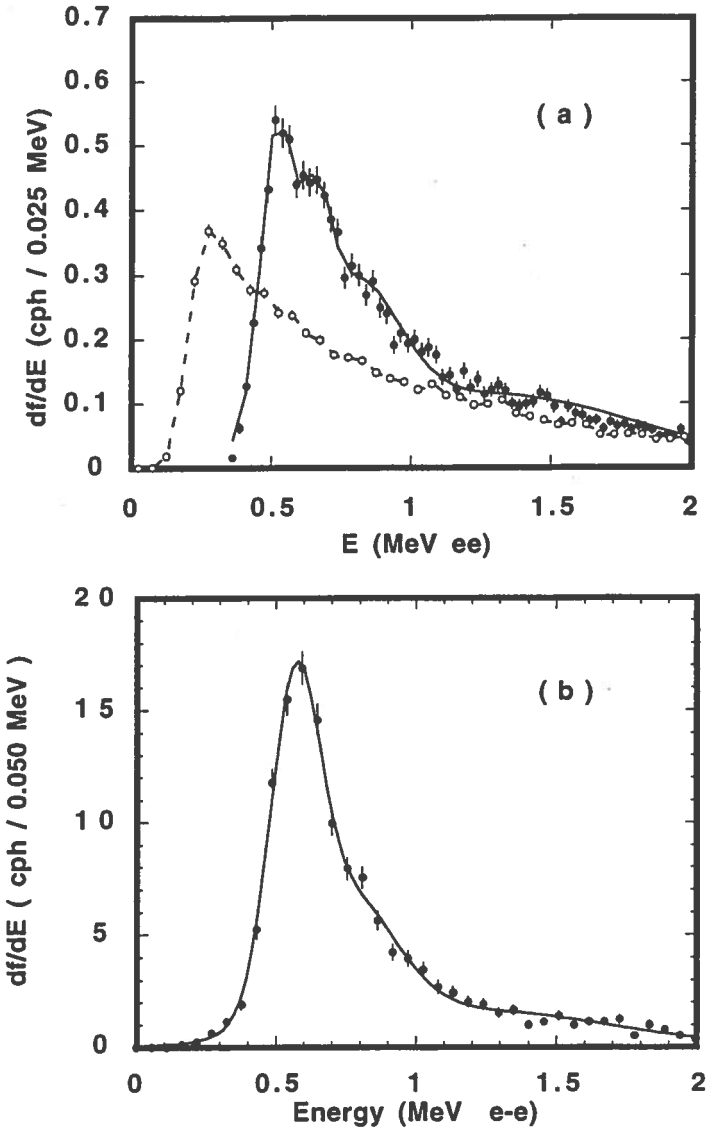


Fig. 7a. The black points represent the energy spectrum (counts per hour), obtained with an aged cell, of the PSD neutron selected sample. For sake of comparison the spectrum of $^{225}Cf$ (white points) is also plotted in arbitrary units.

7b. The energy spectrum (counts per hour) obtained with a counter just filled with scintillator few hours before to run the measure.

The continuous lines represent the best fit described in the text.

An evidence about the nature of these signals came out when we tested the second cell (Cell-1), which had been filled in our laboratory few hours before to start the measurements. The spurious pulses had an energy distribution (Fig. 7b) similar to that shown in Fig. 7a, showing data from the first counter which was put in measure some weeks after being filled with the scintillator. However, the count rate from Cell-1 was much larger and showed a decreasing behavior with time. The rate vs. time is shown in Fig.8.

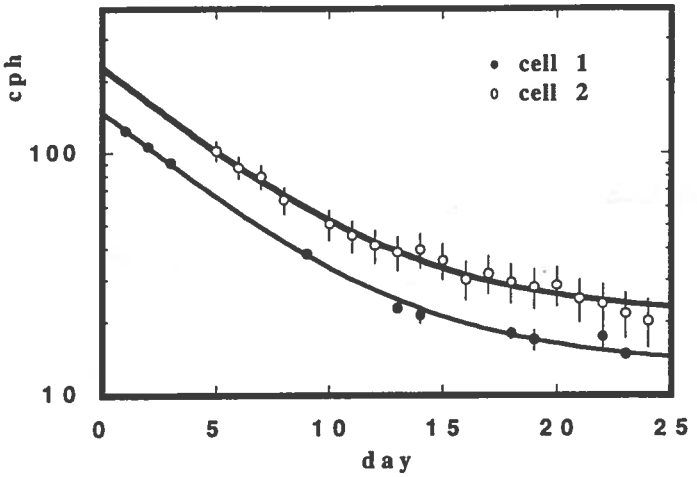


Fig. 8 The rates (counts per hour, *cph*) of two cells as a function of the time. The origin of the time axis corresponds to the filling day of the cells. The continuous lines are the result of a best fit described in the text.

The experimental points can be well fitted with an exponential function superimposed to a constant baseline. The same result was obtained with another "freshly" made cell (cell 2). The parameters of the fit are reported in Table I.

| Table I. $cph = I \exp(-t/\tau) + C$ | | |
|---|---|---|
| | *Cell 1* | *Cell 2* |
| I | 135 ± 2 cph | 207 ± 13 cph |
| $\tau$ | 5.3 ± 0.2 d | 5.3 ± 0.3 d |
| C | 13 ± 1 cph | 21 ± 2 cph |
| $\chi$/d.o.f. | 0.7 | 0.2 |

The mean life values suggest that the recorded events are due to alpha particles emitted in the decay of $^{222}$Rn (mean life-time $\tau$=5.52 d). The last daughters in $^{222}$Rn chain, $^{210}$Pb and $^{210}$Po, have very long half lives but intensity consideration led to exclude that these isotopes are responsible for the constant baseline. Hence a possible interpretation is that two independent kinds of radioactive contamination are present in the cells:

a) Rn introduced probably during the filling operations, which is responsible of the fast decaying component,

b) U or Th present in the counter and/or in the scintillator, which are responsible for the constant base line. A possible Radon diffusion in the scintillator through the O-ring materials has been envisaged. The consistency of this hypothesis will be verified experimentally.

The amount of contamination needed to explain the measured intensities is very small. The relation between the number of radioactive atoms N and the counting rate is:

$$N = \frac{T_{1/2}(\text{hours})}{\ln 2} \cdot \text{cph}$$

If the short living impurity is $^{222}Rn$ ($T_{1/2}$ = 92 h) and if the counting rate is 207 *cph* (in the worst case, see Tab. I), then we find N = $2.7 \times 10^4$ atoms; if the long living one is $^{226}Ra$ ($T_{1/2} = 1.4 \times 10^7$ h) and the counting rate 21 *cph* (in the worst case), then we find N = $4 \times 10^8$ atoms.

These hypotheses have been confirmed by analyzing the energy distribution of the spurious pulses. The relevant α-ray emission from natural radionuclides U, Th and daughters is reported in Tab. II. The energy spectrum of the data shown in Fig. 7-b, is consistent with the presence of the $^{222}Rn$ series inside the liquid.

TABLE II. Alpha-ray emitters in U and Th natural chains.

| Nuclide | Eα MeV | $T_{1/2}$ | Nuclide | Eα MeV | $T_{1/2}$ |
|---|---|---|---|---|---|
| U-238 | 4.2 | $4.5 \times 10^9$ y | Th-232 | 4.0 | $1.41 \times 10^{10}$ y |
| U-234 | 4.8 | $2.47 \times 10^5$ y | Th-228 | 5.4 | 1.91 y |
| Th-230 | 4.7 | $8.0 \times 10^4$ y | Ra-224 | 5.7 | 3.64 d |
| Ra-226 ◊ | 4.8 | $1.6 \times 10^3$ y | Rn-220 | 6.3 | 55.3 s |
| Rn-222 * ◊ | 5.5 | 3.82 d | Po-216 | 6.7 | 0.145 s |
| Po-218 * ◊ | 6.0 | 3.05 m | Bi-212 | 6.1 β=0.34 | 60.6 m |
| Po-214 * ◊ | 7.7 | $1.64 \times 10^{-4}$ s | Po-212 | 8.8 β=0.66 | $3.04 \times 10^{-7}$ s |
| Po-210 ◊ | 5.3 | 138 d | | | |

* radon series
◊ radium series

A convolution fit of three gaussian functions (see continuous line in Fig. 7b) gives the following peak energies:

$$E_1 = 0.565 \pm 0.003 \text{ MeV ee}$$
$$E_2 = 0.740 \pm 0.045 \text{ MeV ee}$$
$$E_3 = 1.211 \pm 0.138 \text{ MeV ee}$$

Assuming that this three peaks belong to the Radon series, we obtain the white circles in the plot of fig. 9, which are compatible with the published data on α particles relative quantum efficiency. The areas below the gaussian functions turn out to be (*cph*):

$$A(^{222}Rn)=55\pm7, \quad A(^{218}Po)=52\pm10, \quad A(^{214}Po)=40\pm5,$$

that are equal within the errors, as should be if the chain members are at the equilibrium.

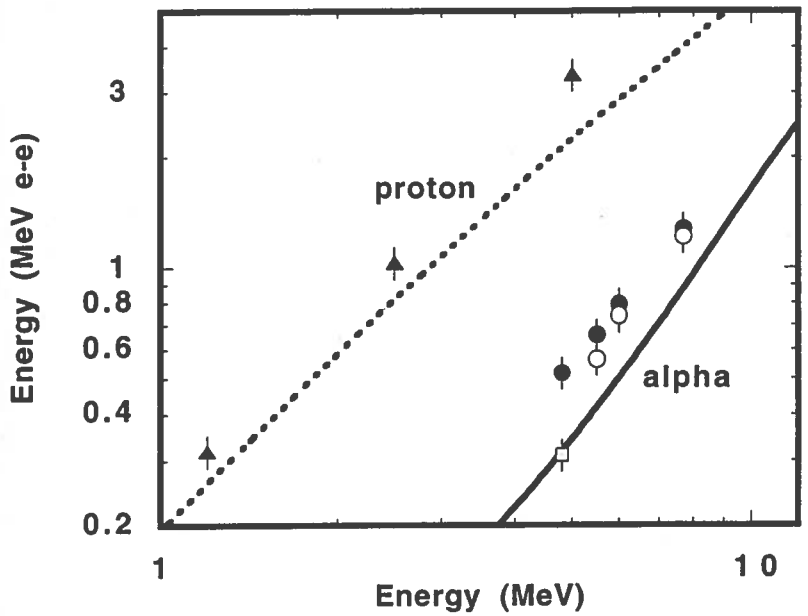


Fig. 9 Correlation between the quantum efficiency of electron and that of protons and α particles. The curves are reported in the literature [6]. The black circles are the result of the best fit with the radium series in the aged cells, whereas the white circles are the result with the radon series in the just filled cells. The squared point is obtained with a $^{234}$U α particle source. The black triangular points are the results of a calibration done with monoenergetic neutron beams [8].

By applying the same fit procedure to the data of Fig. 7a, with four gaussian functions with mean values corresponding to the energy lines of the radium series, we check the hypothesis of an additional $^{226}$Ra contamination surviving the Rn disappearance. The four peak-energies resulting from the fit procedure are:

$$E_1 = 0.518 \pm 0.002 \text{ MeV\_ee}$$
$$E_2 = 0.656 \pm 0.004 \text{ MeV\_ee}$$
$$E_3 = 0.793 \pm 0.006 \text{ MeV\_ee}$$
$$E_4 = 1.275 \pm 0.023 \text{ MeV\_ee}$$

Assuming that this four peak-energies belong to the radium series, we obtain the black circles in the plot of Fig. 9. We don't take into account the Thorium chain because its contamination is usually lower than the Uranium contamination. The areas below the gauss function are (cph):

$$A(^{226}\text{Ra}) = 2.5\pm0.3, \quad A(^{222}\text{Rn}) = 1.2\pm0.4, \quad A(^{218}\text{Po}) = 3.4\pm0.7, \quad A(^{214}\text{Po}) = 6.2\pm1.1$$

We check also the hypothesis of Ra presence in the counter walls. We considered two possibilities:

a) Rn contamination into the liquid due to diffusion from the cell walls

b) $\alpha$ particles generation inside the walls of the detector.

In the first case the result of the best fit with the Radon hypothesis was worse with respect to the radium hypothesis previously discussed. In the second case the spectrum should be strongly degraded due to the energy in the wall material.

We conclude that the PSD selected sample is mainly due to $\alpha$ particle emitters, belonging to the Uranium series, released into the scintillation liquid.

## 6. Conclusions

The presence of $\alpha$ particle emitters in the liquid scintillator counters, explains the nature of the non-neutron signals surviving the selection with the PSD technique. For what concern a neutron flux measurement in the hall-C, the background, discussed in the previous paragraph, must to be cut. As said above the additional condition consists in the detection of a delayed $\gamma$-ray from n-capture. With the full 32-cell-device a satisfactory rejection of spurious events will be achieved. The net number of proton recoils associated with a delayed capture gamma ray, recorded in our test run ($2.6 \times 10^6$ s), is consistent with a neutron flux less than $10^{-2}$ n/s $m^2$. The final detector efficiency will be about 40 times greater, therefore we will collect a sample of about thousand unambiguous neutrons in 100 days run, leading to a statistical error less than 3% in the flux.

## Acknowledgments

We would like to thank O.Barnabà, G.Musitelli, from the Electronic Workshop of the Pavia Physics Department, and B. Romualdi, from the Mechanical Workshop of the Gran Sasso Laboratory, for their skilled work and precious help in preparing the neutron detector used during this test. We would also like to express our thanks to L. Periale for his important support and suggestions on many aspects of the liquid scintillator techniques.

**References**

[1] - ICARUS Collaboration, "ICARUS II: second generation proton decay experiment and neutrino observatory at the Gran Sasso Laboratory", Proposal Vol. I & Vol. II, **LNGS-94/99** (1994).
- ICARUS Collaboration: "A first 600 ton ICARUS detector installed at the Gran Sasso Laboratory", Addendum to the Proposal, **LNGS-94/99** (1996).

[2] - P. Belli et al., *Il Nuovo Cimento* **101 A 6** (1989), 959.
- R. Aleksan et al., *Nucl. Instr. and Meth.* **A 274** (1989), 203.
- E. Bellotti et al., **INFN/TC-85/19** (1985).

[3] - ICARUS Collaboration: "Study of solar neutrino detection in the 600 liquid argon ICARUS time projection chamber", **ICARUS TM 97/05** (1997).

[4] - O. Barnaba' et al., "A Full-Integrated Pulse Shape Discriminator for Liquid Scintillator Counters", **ICARUS-TM-97/04** (1997).

[5] - A.Bertin et al., *Nucl. Instr. and Meth.* **A 337** (1994), 445.

[6] - C.L.Morris et al. Nucl. Instr. and Methods 137 (1976), 397.

[7] - R.A. Cecil et al., *Nucl. Instr. and Meth.* **161** (1979), 439.
(*BC501A* liquid scintillator reference sheets).

[8] - F. Arneodo et al. , "Calibration of BC501A liquid scintillator cells with monochromatic neutron beam", **ICARUS-TM-97/8** (1997).

[9] - A. Bertin, A. Vitale and A. Placci, *Nucl. Instr. and Meth.* **91** (1971), 649.